conformational and X-ray studies, is such that the imino group is less readily accessible for intermolecular interactions than the carboxyl group. Indeed the former is not involved in intermolecular interactions in any of the relevant crystal structures whereas the latter is in all of them. Therefore, the carboxyl group is the only common site of specific interaction in all the fenamates. Thus, an important role of the carboxyl group would appear to be as a site for intermolecular interactions. As noted earlier, it also helps stabilize the invariant coplanar feature in the molecule, in addition to endowing hydrophilicity to one end of the molecule.

Molecular asymmetry

Seven out of the eight crystals containing fenamate molecules studied so far are centrosymmetric. In the eighth, there are two molecules in the asymmetric unit, related to each other by a pseudo-inversion centre. Thus in every crystal, half of the molecules are related to the other half by an inversion centre. This is hardly surprising since they do not contain chiral centres, nor do they have any obvious overall asymmetry. However, it was observed that the molecule and its inversion equivalent are non-superimposable. Thus, they are asymmetric and the crystals contain a *racemic* mixture. As can be seen from Table 1, for all practical purposes, the torsion angle θ_3 can be approximated to 0° and θ_1 to 180° in all fenamates. Thus the two isomers of a given fenamate molecule can be differentiated essentially by the sign of θ_2. In the conformational energy maps of all the fenamates except niflumic acid, the main allowed regions corresponding to the positive and negative values of θ_2 are separated by a disallowed region (energy greater than 5 kcal mol^{-1}). The strategy adopted in the conformational analysis does not permit the evaluation of the actual potential-energy barrier between the regions. Hence, it cannot yet be ascertained whether rapid interconversion between the two isomers is possible. Thus, the physiological role, if any, of the observed asymmetry needs further elucidation.

The authors thank the University Grants Commission, India, for support.

References

BRANT, D. A. & FLORY, P. J. (1965). *J. Am. Chem. Soc.* **87**, 663–664.

CURL, R. F. (1959). *J. Chem. Phys.* **30**, 1529–1536.

CUSHMAN, D. W. & CHEUNG, H. S. (1976). *Biochim. Biophys. Acta*, **424**, 449–459.

DEL RE, G. (1958). *J. Chem. Soc.* pp. 4031–4040.

DHANARAJ, V. & VIJAYAN, M. (1983). *Acta Cryst.* C**39**, 1398–1401.

DHANARAJ, V. & VIJAYAN, M. (1987). *Biochim. Biophys. Acta*, **924**, 135–146.

DONOHUE, J., LAVINE, L. R. & ROLLET, J. S. (1956). *Acta Cryst.* **9**, 655–662.

FLOWER, R. J. (1974). *Pharmacol. Rev.* **26**, 33–67.

HOPFINGER, A. J. (1973). In *Conformational Properties of Macromolecules*. New York: Academic Press.

KRISHNA MURTHY, H. M., BHAT, T. N. & VIJAYAN, M. (1982). *Acta Cryst.* B**38**, 315–317.

KRISHNA MURTHY, H. M. & VIJAYAN, M. (1979). *Acta Cryst.* B**35**, 262–263.

KRISHNA MURTHY, H. M. & VIJAYAN, M. (1981*a*). *Acta Cryst.* B**37**, 210–213.

KRISHNA MURTHY, H. M. & VIJAYAN, M. (1981*b*). *Acta Cryst.* B**37**, 1102–1105.

KRISHNA MURTHY, H. M., VIJAYAN, M. & BREHM, L. (1979). *Acta Cryst.* B**35**, 612–615.

MCCONNELL, J. F. (1973). *Cryst. Struct. Commun.* **2**, 459–461.

MCCONNELL, J. F. & COMPANY, F. Z. (1976). *Cryst. Struct. Commun.* **5**, 861–864.

PAULING, L. (1960). In *The Nature of the Chemical Bond*. Ithaca: Cornell Univ. Press.

PULLMAN, B. & PULLMAN, A. (1963). In *Quantum Biochemistry*. London: Interscience.

SIMON, Z. (1973). In *Quantum Biochemistry and Specific Interactions*. Tunbridge Wells, UK: Abacus Press.

SINGH, T. P. & VIJAYAN, M. (1974). *Acta Cryst.* B**30**, 557–562.

SINGH, T. P. & VIJAYAN, M. (1977). *J. Chem. Soc. Perkin Trans.* 2, pp. 693–699.

VIJAYAN, M. (1983). *Proc. Indian Acad. Sci. (Chem. Sci.)*, **92**, 463–471.

Acta Cryst. (1988). B**44**, 412–426

Static Deformation Densities for Cytosine and Adenine

BY MIRIAM EISENSTEIN

Department of Structural Chemistry, The Weizmann Institute of Science, Rehovot 76100, *Israel*

(*Received* 17 *September* 1987; *accepted* 29 *February* 1988)

Abstract

X-ray diffraction intensities for cytosine monohydrate have been measured at 97 K, to $2\sin\theta/\lambda = 2{\cdot}74$ Å^{-1}, and used in a deformation refinement. Crystal data for cytosine monohydrate at 97 K: $a = 7{\cdot}728\ (1)$, $b = 9{\cdot}817\ (3)$, $c = 7{\cdot}520\ (1)$, $\beta = 100{\cdot}50°$, $V = 560{\cdot}94$ Å^3, $R = 0{\cdot}0341$ for 6456 unique reflections. The experimental static deformation density of cytosine compares very well with the corresponding theoretical

0108-7681/88/040412-15$03.00

4-31G** deformation density. Differences between theory and experiment occur at hydrogen-bonding sites. They are very similar to the corresponding differences between the theoretical deformation densities of formic acid monomer and cyclic dimer. The experimental static deformation density of 9-methyladenine was obtained in a deformation refinement against the low-temperature X-ray data of Craven & Benci [*Acta Cryst.* (1981), B**37**, 1584–1591]. It is similar to the maps presented by these authors. The comparison of the experimental deformation density of 9-methyladenine with the theoretical 4-31G deformation density of adenine shows qualitative agreement, which is improved when the 4-31G results are corrected for the absence of polarization functions in the basis set. Some of the remaining differences reflect the effects of substituting CH_3 for H. The weak N···H hydrogen bonds have little influence on the deformation density in this structure.

Introduction

Molecular charge distributions can be partitioned into atomic fragments and described quantitatively by atomic multipole moments (*e.g.* Hirshfeld, 1977*a*; Bader & Beddall, 1972; Bader, Beddall & Peslak, 1973). Such moments permit the calculation of electrostatic potentials around molecules and electrostatic interaction energies between molecules (*e.g.* Hirshfeld & Mirsky, 1979). Atomic multipole moments derived from experimental deformation densities have been used successfully for predicting crystal-packing motifs (Berkovitch-Yellin & Leiserowitz, 1980, 1982). This is particularly important for large molecules, where *ab-initio* computations giving good approximations to the molecular charge density require large basis sets and may be prohibitively long. Thus, we have undertaken an experimental study of the electron densities in DNA bases and a theoretical study of transferability between such molecules (Eisenstein, 1988). Comparison of the experimental and theoretical results may serve to establish the accuracy of both and to produce a combined set of atomic multipole moments for estimation of electrostatic interaction energies within the DNA double helix.

Several X-ray and neutron studies on purines and pyrimidines have been published. These include a low-temperature study of the deformation density in 9-methyladenine (Craven & Benci, 1981). We have crystallized cytosine monohydrate and determined the static electron distributions in the cytosine and water molecules in this structure. In addition, we have obtained the intensity data for 9-methyladenine from SUP 35971 and used it to derive the static deformation density in this compound. Thus, we report the electron distributions in one purine and one pyrimidine. From these it is possible to approximate charge densities and electrostatic potentials of similar molecules (Eisenstein, 1988).

Experimental

Crystals of cytosine monohydrate were grown from an aqueous solution by slow evaporation at room temperature. The crystal chosen for the experiment was elongated and had dimensions $0{\cdot}3 \times 0{\cdot}3 \times 10$ mm. It was cleaved by touching delicately with a blade, producing a specimen of $\sim 0{\cdot}3$ mm in the third dimension as well. The room-temperature crystal parameters were $a = 7{\cdot}791$, $b = 9{\cdot}824$, $c = 7{\cdot}669$ Å and $\beta = 99{\cdot}51°$, in accord with the monoclinic $P2_1/c$ structure of cytosine monohydrate (Niedle, Achari & Rabinovitch, 1976).

X-ray intensities were measured on a Nonius CAD-4 diffractometer equipped with a cooling device. In several cooling attempts the crystals either cracked or underwent a phase transition, in one case producing a structure with a cell volume 16 times the room-temperature value [$a = 18{\cdot}46$ (1), $b = 20{\cdot}59$ (1), $c = 24{\cdot}99$ (1) Å, $\alpha = 93{\cdot}36$ (4), $\beta = 104{\cdot}65$ (3), $\gamma = 100{\cdot}75$ (4)°, $V = 8975{\cdot}1$ Å^3]. In another case, shock cooling to 97 K left the crystal in a metastable form, which was used for data collection. The cell parameters $a = 7{\cdot}728$ (1), $b = 9{\cdot}817$ (3), $c = 7{\cdot}520$ (1) Å, $\alpha = 90{\cdot}00$ (2), $\beta = 100{\cdot}50$ (1), $\gamma = 90{\cdot}01$ (2)°, $V = 560{\cdot}94$ Å^3 have been determined from the diffractometer angles of 25 reflections with $24 \le \theta \le 33°$ (Mo $K\alpha$ radiation). These are close to the room-temperature values. The long-term fluctuations in the temperature were $\pm 0{\cdot}5$ K. After data collection the temperature was raised gradually. The cell parameters at ~ 140 K, determined from the diffractometer angles of 12 reflections with $11 \le \theta \le 17°$, were $a = 6{\cdot}940$ (6), $b = 7{\cdot}557$ (4), $c = 7{\cdot}642$ (5) Å, $\alpha = 54{\cdot}28$ (5), $\beta = 63{\cdot}83$ (7), $\gamma = 63{\cdot}57$ (5)°, $V = 282{\cdot}2$ Å^3, about half the monoclinic cell volume. The matrix ($\bar{1}00$, $0\bar{1}1$, 011) applied to this unit cell produces a hexagonal cell [$a = 6{\cdot}940$ (6), $b = 6{\cdot}934$ (3), $c = 13{\cdot}525$ (9), $\alpha = 89{\cdot}21$ (5), $\beta = 119{\cdot}86$ (6), $\gamma = 90{\cdot}06$ (5), $V = 564{\cdot}4$ Å^3]. At a higher temperature the crystal became opaque, few reflections could be found, and these had very wide profiles.

Data collection at 97 K proceeded in two steps. First, reflections with $\theta < 27°$ were scanned. Three minutes at most were allotted for each scan. These data were used in a preliminary refinement, including a deformation model (see below). Structure factors were then computed for the remaining reflections up to $\theta = 77°$ ($S = 2\sin\theta/\lambda = 2{\cdot}74$ Å^{-1}). In this range only those reflections were scanned where $I > 2\sigma(I)$ (h −21–9, k 0–26, l 0–20). For $\theta > 60°$, the maximum time allotted per scan was seven minutes.

The 005 reflection showed some net intensity despite the space-group absences. However, rotation about the

reflection vector **S** in either direction was enough to lose this intensity peak, suggesting a multiple-reflection effect (Coppens, 1968). Therefore, the strongest 150 reflections were listed and the possibility of multiple reflections at the expected crystal orientation was checked. The several reflections which the computer had flagged (including 005) were remeasured after rotation about **S**.

The measured intensities were corrected for Lorentz and polarization factors and for absorption (Coppens, Leiserowitz & Rabinovich, 1965). The largest and smallest transmission factors differed by only 1%. The initial variances were based on the counting statistics plus a 2% error in I. The number of unique reflections was 6456. The histogram in Fig. 1 shows their number as function of $\sin\theta$. The large proportion of high-order reflections is encouraging as it permits the successful separation of the effects of atomic vibrations and chemical bonding on the molecular charge density (Hirshfeld, 1976).

Refinement for cytosine monohydrate

Initial parameters

The starting positional and thermal parameters were taken from the low-temperature neutron structure of deuterated cytosine monohydrate (Weber, Craven & McMullan, 1980). The H-atom coordinates were transformed to local coordinate systems where the X–H bond lengths (X = C, N, O) could be constrained (Hirshfeld, 1977*b*).

The thermal motion of the H atoms cannot be derived accurately from X-ray diffraction data (Hirshfeld, 1976). Therefore, it has been estimated as the sum of two contributions: the motion of a rigid body to which the H atoms are attached and the additional motion of the H atoms relative to that rigid body. The five cytosine H atoms were attached to a skeleton comprising the eight C,N,O atoms of this molecule. The **T**, **L** and **S** tensors of the rigid-body motion of the latter were determined in a constrained refinement and used only for estimating the H-atom vibrations. They were readjusted as the refinement proceeded. The mean-square stretching and in-plane bending displacements for the cytosine H atoms could be estimated from the vibrational spectrum of this molecule (Susi, Ard & Purcell, 1973). The internal vibration parameters for H5 and H6, which were not replaced by deuterium in the neutron diffraction experiment (Weber, Craven & McMullan, 1980), could be estimated also from the difference between their U_{ij} in the neutron refinement and the computed rigid-body contribution to these quantities. The two estimates for the stretching and in-plane bending of H5 and H6 were close. Thus, the spectroscopic estimates were used for these amplitudes for all the cytosine H atoms. The vibration spectrum also provided mean-square out-of-plane bending displacements for the NH_2 H atoms. For H1 this parameter was assumed to be equal to the in-plane bending amplitude and the values for H5 and H6 were estimated from the results of the neutron diffraction study as described above. All are listed in Table 1.

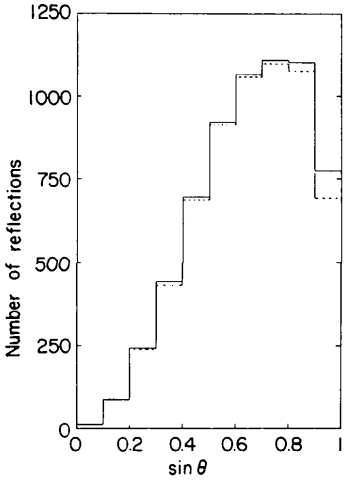

Fig. 1. Number of reflections in small intervals in $\sin\theta$ for cytosine monohydrate. The dashed lines indicate number of reflections with $F_o > 2\sigma(F_o)$.

Table 1. *Cytosine monohydrate – excess mean-square displacements for* H *atoms* (Å^2)

	Stretching	In-plane bending*	Out-of-plane bending*
H1	0·0053	0·011	0·011
H41	0·0051	0·010	0·017
H42	0·0051	0·010	0·017
H5	0·0054	0·010	0·017
H6	0·0054	0·010	0·005
H*W*1	0·0047	0·020	0·021
H*W*2	0·0047	0·020	0·021

* For H*W*1 and H*W*2 these include in-plane and out-of-plane libration (Hermansson & Lunell, 1982).

The thermal motion of the water H atoms has been approximated similarly, by combining their librational and internal vibrations with the motion of O*W*. It was necessary to estimate the excess motion of the H atoms relative to this O atom, along the O–H bond and transverse to the bond in the H_2O plane and perpendicular to this plane. The relative mean-square displacements for D_2O have been calculated from the results of the low-temperature neutron study of deuterated cytosine monohydrate (Weber, Craven & McMullan, 1980). This gave 0·0030 Å^2 on average for the mean-square stretching amplitudes of D*W*1 and D*W*2, 0·013 Å^2 for the in-plane libration plus bending, and 0·010 Å^2 for the total out-of-plane libration. These values for D_2O were corrected for the difference in motion between deuterium and hydrogen, estimated from the ranges of mean-square displacements in the

appropriate modes of D_2O and H_2O (Eriksson & Hermansson, 1983). The excess vibration parameters for the water H atoms are also listed in Table 1.

Deformation refinement

Hirshfeld's (1977*b*) deformation model has been used in the refinement. In this model the molecular deformation density ($\delta\rho$; molecule minus sum of spherical-atom distributions) is described as a sum of atom-centered multipoles of the general form:

$$\rho_{a,n,k}(\mathbf{r}) = N_n r_a^n \exp(-\alpha_a r_a) \cos^n(\theta_{a,\mathbf{k}})$$

where a indicates an atomic center, n accepts integer values from 0 to 4, r_a is the distance of point $\mathbf{r}$ from the nucleus a, α_a is a shape parameter that can be refined and is common to all the deformations on a particular atom (except for the $\rho_{a,0}$ functions; see below), $\mathbf{k}$ denotes an axis passing through the nucleus, $\theta_{a,\mathbf{k}}$ is the angle between the vector $\mathbf{r}$ and the axis $\mathbf{k}$, and N_n is a normalizing factor that depends on α_a. It is possible to specify 35 deformation functions for each atom and to refine 36 parameters: 35 deformation coefficients and the value of α_a. However, initially several constraints were imposed on the deformation parameters. Thus, there were ten deformation types, one for each C,N,O atom and one common to all the H atoms. The deformations of the C,N,O atoms were constrained to *mm* symmetry and the coefficients of their cusp functions ($\rho_{a,0}$) were fixed at 0. The H atoms were contracted to an effective nuclear charge of $\zeta = 1{\cdot}2$ (Harel & Hirshfeld, 1975) and their deformations had axial symmetry. Also, because of the necessary approximations in the vibrational model for the H atoms, their deformations were limited to $n \leq 3$. Neutrality of the system was maintained by fixing the value of $F(000)$ at the number of electrons in the unit cell (Harel & Hirshfeld, 1975).

With this model 224 parameters were refined: 81 positional and anisotropic thermal parameters for the C,N,O atoms and 14 coordinates for the H atoms (fixed X—H bond lengths and internal vibration amplitudes), 123 deformation coefficients and four α_a, one for each group C,N,O,H, a scale factor and an isotropic extinction parameter. The value of the latter, $c = 0{\cdot}0031$, was determined by trial and error. It increased the scaled F_o's for strong reflections according to $(F_o)_{\text{corr}} = F_o/(1 - c^2F_o^2)$. The largest corrections were 19·7 and 5·4% of F_o for the 102 and 104 reflections, respectively. With this approximate extinction correction it was necessary to reduce the weights of the strong reflections. The corrected variances had the form $\sigma^2(F^2) = \sigma^2(F_o^2) + (0{\cdot}019F^2)^2 + (0{\cdot}0025F^2)^4$, where $\sigma^2(F_o^2)$ was the initial variance. The coefficient of the second term was determined by trial and error. The coefficient of the last term was chosen to increase $\sigma^2(F^2)$ by the square of one-third of the extinction correction to F_o^2. The program minimizes the quantity $\Delta = \sum w(F_o^2 - k^2F_c^2)^2$ with $w = 1/\sigma^2(F^2)$. The agreement factors obtained with this model were: $R(F) = \sum|F_o - k|F_c|\,|/\sum F_o = 0{\cdot}0344$, $wR(F^2) = [\Delta/\sum wF_o^4]^{1/2} = 0{\cdot}0648$, $G = [\Delta/(n-p)]^{1/2} = 1{\cdot}208$.

Several attempts were made to relax the various constraints imposed on the deformation model. A refinement with separate deformation types for the H_N, H_C and H_O atoms did not reduce wR significantly and the values of $\alpha(H_O)$ increased sharply. Also, refining the in-plane and out-of-plane bending parameters of the H atoms, which may be more sensitive to the environment than the X—H stretching, did not affect wR. However, refining the cusp coefficients for the C,N,O atoms while imposing the theoretical cusp constraint on the values of α_a for the $\rho_{a,0}$ functions (Eisenstein, 1979), added nine parameters and produced a small drop in wR and G to 0·0647 and 1·207, respectively. This drop was significant according to Hamilton's (1965) test. In the latter refinement $\zeta_H = 1{\cdot}0$ for consistency with the cusp constraint.

Next, several relaxations of the symmetry constraints were tested. Lowering the symmetry of the deformations on any atom from *mm* to *m* added eight parameters to the refinement. Such a change for N3, C4 or C5 did not produce a significant drop in wR. However, similar treatments for N1, C2 and C6 lowered wR very slightly but significantly. The carbonyl and water O atoms are involved in hydrogen bonds which do not comply with the molecular symmetry. Therefore, the deformations of these two atoms were refined without any symmetry restrictions. This added 21 parameters for each atom and produced a considerable lowering of wR. A similar check for N4 showed that symmetry changes for this atom were unnecessary. Separating the α_a parameters for the several atoms produced a significant change only for the O atoms. However, α_{O2} did not refine well and obtained an unreasonably high value. This constraint ($\alpha_{O2} = \alpha_{Ow}$) was the only one that had to be retained for the deformations of the C,N,O atoms. Finally, 299 parameters were refined, producing $R = 0{\cdot}0341$, $wR = 0{\cdot}0634$ and $G = 1{\cdot}192$.

Structure and deformation density of cytosine monohydrate

Atomic positions and thermal vibrations

The coordinates and thermal parameters from the final refinement for cytosine monohydrate are listed in Table 2.* The atomic positions are very close to the

* A list of structure factors has been deposited with the British Library Document Supply Centre as Supplementary Publication No. SUP 44811 (20 pp.). Copies may be obtained through The Executive Secretary, International Union of Crystallography, 5 Abbey Square, Chester CH1 2HU, England.

Table 2. *Cytosine monohydrate – atomic fractional coordinates and anisotropic thermal parameters* $\times 10^5$ (Å^2)

Atom labels are indicated in Figs. 2(*a*) and 2(*b*)

	x	y	z	U_{11}	U_{22}	U_{33}	U_{12}	U_{13}	U_{23}
N1	8513 (7)	434 (5)	21867 (4)	1049 (12)	673 (11)	1380 (16)	25 (7)	438 (9)	15 (6)
C2	196 (5)	12503 (5)	23997 (4)	913 (9)	718 (10)	1143 (12)	28 (7)	370 (7)	−1 (7)
O2	−14822 (8)	12087 (7)	28284 (9)	1076 (13)	1050 (13)	1731 (19)	14 (10)	673 (11)	27 (12)
N3	7914 (4)	24442 (4)	21093 (4)	965 (10)	678 (10)	1328 (15)	38 (6)	434 (8)	8 (6)
C4	23587 (4)	24326 (4)	15680 (4)	954 (10)	715 (10)	1181 (13)	25 (7)	366 (8)	14 (6)
N4	31104 (4)	36214 (5)	13104 (4)	1193 (11)	797 (11)	1888 (19)	−74 (7)	645 (10)	37 (7)
C5	32211 (5)	11868 (3)	12615 (4)	1104 (10)	845 (11)	1588 (15)	70 (6)	598 (9)	−23 (7)
C6	24192 (6)	154 (5)	16055 (4)	1135 (12)	755 (11)	1418 (15)	113 (7)	478 (9)	−39 (7)
OW	−35391 (9)	29108 (7)	2535 (9)	1209 (15)	1481 (17)	1645 (20)	78 (11)	548 (12)	126 (13)
H1	2148	−8391	24642	2280	1431	2714	−273	770	165
H41	42814	36153	8829	2116	2037	3981	−176	1524	86
H42	25175	44995	15996	2498	1380	3820	93	1250	−60
H5	44591	12172	7887	2028	2086	3815	87	1559	−50
H6	29667	−9845	14260	2245	1407	2756	366	718	−161
HW1	−27083	32496	−4592	2131	3192	2860	−51	1081	602
HW2	−28199	23729	11838	2342	3088	2896	412	449	874

Table 3. *Cytosine monohydrate – mean-square displacements of bonded atoms along the bonds* $\times 10^5$ (Å^2)

R.m.s. difference 0·00025 Å^2.

A–*B* bond	Z_A^2	Z_B^2	*A*–*B* bond	Z_A^2	Z_B^2
N1–C2	716	711	C4–N4	757	759
C2–O2	785	793	C4–C5	730	775
C2–N3	756	739	C5–C6	914	922
N3–C4	809	828	N1–C6	894	941

corresponding parameters from the neutron diffraction study (Weber, Craven & McMullan, 1980). However, the U_{ii} ($i = 1, 3$) in Table 2 are consistently larger than in the neutron study, by 0·0025 Å^2 on average. This may be due to the difference in temperature of ~15 K.

The mean-square displacements of bonded atoms along the bonds are listed in Table 3. The differences are all small as required by the rigid-bond test (Hirshfeld, 1976).

Experimental deformation density

The experimental deformation density in the mean plane of the cytosine molecule and in sections perpendicular to this plane is plotted in Figs. 3–6 and the $\delta\rho$ for water appears in Fig. 7. The heavy contours around the C,N,O positions surround regions where $\sigma(\delta\rho) > 0{\cdot}1$ e Å^{-3}. At the H-atom positions $\sigma(\delta\rho) = 0{\cdot}08$ e Å^{-3}. In the bonding regions the error is much smaller. Thus, at the bond peaks it reaches 0·02 e Å^{-3}, except for the N1–H1, C4–N4 and C6–H6 bond peaks where $\sigma(\delta\rho) = 0{\cdot}03$ e Å^{-3}. At the ring center $\sigma(\delta\rho) = 0{\cdot}01$ e Å^{-3}.

The deformation density has been partitioned into atomic fragments (Hirshfeld, 1977*a*) and integrated. The integration was carried out on an 0·2 Å rectangular grid, except for the cusp regions, where a grid of 0·04 Å was used. The resultant atomic charges, dipole moments and second moments for cytosine and water are listed in Table 4 and 5 in the local coordinate systems shown in Figs. 2(*a*) and 2(*b*). The sum of the net atomic charges for each of the two molecules is zero within the integration error, indicating no charge transfer between them.

Figures 3(*a*), 4(*a*) and 7 show large peaks between every pair of bonded atoms and non-bonding density peaks near O2, O*W* and N3. The latter atoms have

Table 4. *Cytosine – experimental and theoretical (Eisenstein, 1988) atomic multipole moments* $\times 10^3$ (e, e Å, e Å^2)

Local coordinate systems are indicated in Fig. 2(*a*).

	Basis	q	μ_l	μ_m	μ_n	μ_{ll}	μ_{mm}	μ_{nn}	μ_{lm}	μ_{ln}	μ_{mn}
N1	Exp.	−67	−11	7	−2	86	58	77	6	−1	−1
	4·31G**	−66	4	7	0	88	64	25	5	0	0
C2	Exp.	158	36	−34	−8	33	38	184	5	4	1
	4·31G**	229	55	−32	0	25	31	184	3	0	0
O2	Exp.	−311	68	−6	−5	−58	−41	−34	−1	5	−1
	4·31G**	−442	99	4	0	−69	127	−100	−3	0	0
N3	Exp.	−233	105	6	1	−43	16	20	−12	0	0
	4·31G**	269	154	−10	0	−99	18	−57	−9	0	0
C4	Exp.	135	−20	8	−3	77	48	212	−7	0	1
	4·31G**	168	−24	13	0	64	38	161	−7	0	0
N4	Exp.	−91	−12	5	4	76	77	65	2	−1	−2
	4·31G**	−140	2	3	0	71	85	−20	3	0	0
C5	Exp.	−92	5	−18	−2	54	81	122	2	0	0
	4·31G**	−117	−15	−33	0	82	73	46	−7	0	0
C6	Exp.	67	−21	−35	1	91	72	206	−13	1	0
	4·31G**	83	−31	−58	0	115	60	152	−15	0	0
H1	Exp.	132	−45	−2	1	10	57	55	−1	2	0
	4·31G**	157	−112	−7	0	94	88	82	3	0	0
H41	Exp.	110	−43	2	0	6	59	47	−2	−1	−1
	4·31G**	135	−109	4	0	88	96	73	−1	0	0
H42	Exp.	108	−42	7	−3	−4	51	42	4	2	−1
	4·31G**	147	−112	11	0	91	86	74	−3	0	0
H5	Exp.	23	−33	−7	−2	−10	45	29	0	−1	0
	4·31G**	39	−85	−1	0	64	80	57	0	0	0
H6	Exp.	60	−29	−1	1	−2	51	50	−2	2	0
	4·31G**	70	−86	0	0	74	90	81	−1	0	0

Table 5. *Cytosine monohydrate – atomic multipole moments for water* O *and* H *atoms* $\times 10^3$ (e, e Å, e Å^2)

Local coordinate systems are indicated in Fig. 2(*b*).

	Basis	q	μ_l	μ_m	μ_n	μ_{ll}	μ_{mm}	μ_{nn}	μ_{lm}	μ_{ln}	μ_{mn}
O*W*	Exp.	−258	97	17	3	−17	29	−19	−12	−4	9
	4·31G**	−339	96	0	0	−38	41	−90	0	0	0
HW1	Exp.	128	−47	8	1	−29	39	23	8	6	3
	4·31G**	168	−120	5	0	−89	109	92	6	0	0
HW2	Exp.	135	−51	13	1	−23	30	25	8	3	−1
	4·31G**	168	−120	5	0	−89	109	92	6	0	0

large dipole moments pointing away from their non-bonding peaks and they expand in the same direction (Table 4). The water O atom is less negative and expands less than O2 (Table 5). A section through the non-bonding density peak near O2, perpendicular to the C2–O2 axis and 0·1 Å behind the O atom (Fig. 5), shows an approximately circular charge distribution suggesting some C–O$^-$ character to this bond.

Comparison of the width of each peak in the molecular plane of cytosine (Fig. 3*a*) and in the perpendicular plane (Fig. 4*a*) shows that all eight bond peaks in the C,N,O skeleton are elongated in the out-of-plane direction. The latter sections also show negative densities above and below each C atom, indicating transfer of π charge into the bonds. This is expressed quantitatively by the anisotropy of their seond moments: $\mu_{nn} \gg \mu_{ll}, \mu_{mm}$ (Table 4). C5 is less contracted than the other C atoms in the *n* direction and has much shallower troughs, as in the theoretical maps (Fig. 4). The regions above and below the nitrogens (Fig. 4*a*) are positive especially near N4, because these atoms bear non-bonding $p\pi$ density.

The H atoms are all positively charged. However, those attached to N or O are appreciably more positive than the –CH– H atoms, as in the theoretical results (Table 4). All the H atoms have negative μ_l, indicating charge migration from behind the atom into the *X*–H bond. This charge polarization is clearly observed in the maps as shallow troughs behind the H atoms and large bonding peaks encompassing the nuclei. The H atoms are contracted, with $\mu_{ll} \ll \mu_{mm} \approx \mu_{nn}$. This anisotropy is related to hydrogen bonding (see below).

Sections through the hydrogen bonds are plotted in Fig. 6. O2 participates in three hydrogen bonds: to H*W*1 (x, $\frac{1}{2}-y$, $\frac{1}{2}+z$), 28° below the molecular plane, to H*W*2 (x, y, z), 48° above the molecular plane, and to

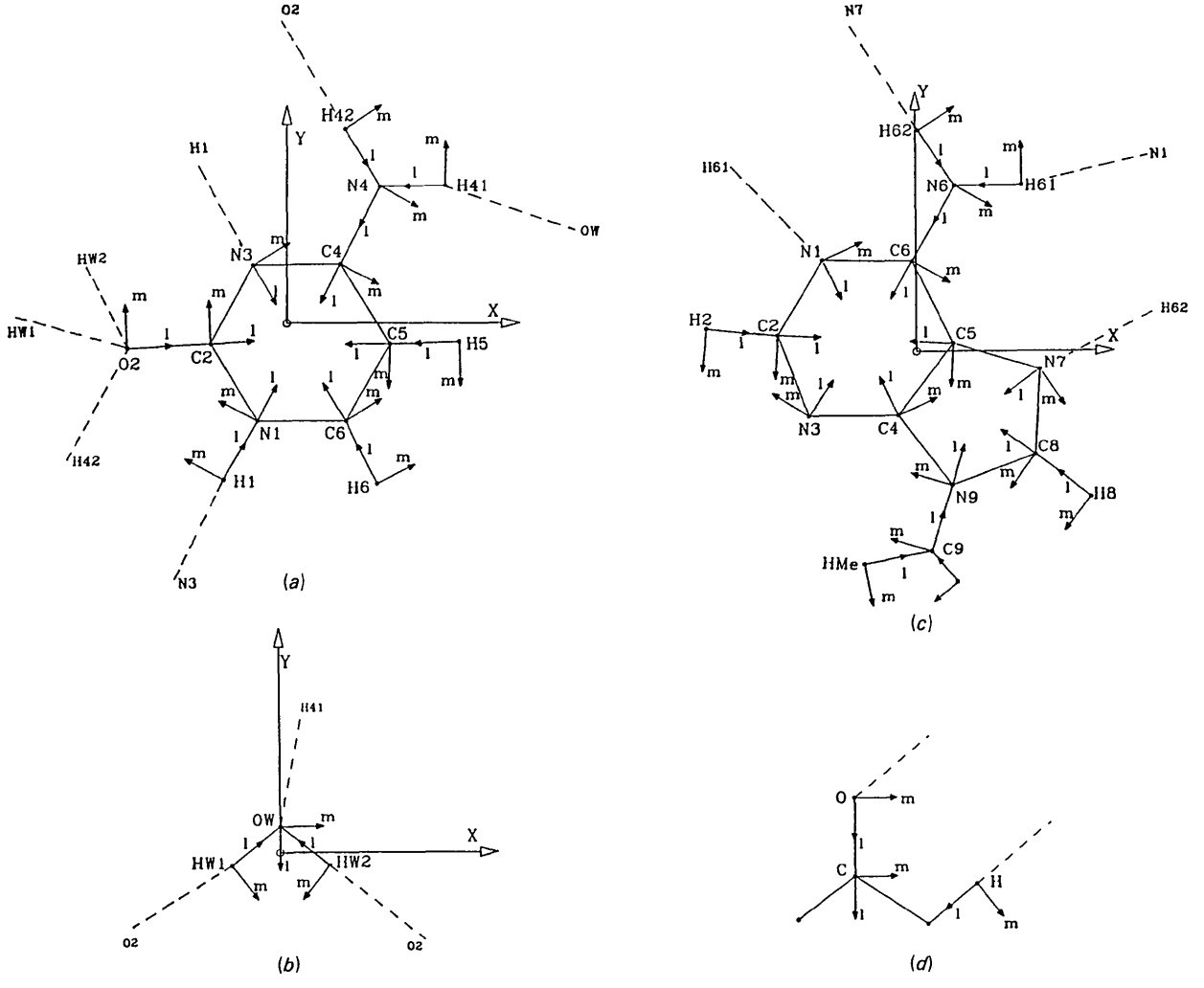

Fig. 2. Local *l,m,n* coordinate systems. Molecular *x,y,z* coordinate systems are indicated for cytosine, water and 9-methyladenine. The *n* and *z* axes are perpendicular to the molecular planes. The dashed lines indicate hydrogen bonds in the cytosine monohydrate and 9-methyladenine crystals and in formic acid cyclic dimer. (*a*) Cytosine, (*b*) water, (*c*) 9-methyladenine, (*d*) formic acid.

H42 ($-x$, $-\frac{1}{2}+y$, $\frac{1}{2}-z$), in the plane. The non-bonding density of O2 is polarized toward the shortest hydrogen bond to H*W*1 (Fig. 6*a*). N3 is hydrogen bonded to H1 ($-x$, $\frac{1}{2}+y$, $\frac{1}{2}-z$), in the molecular plane. H41 interacts with O*W* ($1+x$, y, z), and H5 and H6 participate in very weak C—H···O interactions with O*W* ($1+x$, y, z) and O*W* ($-x$, $-y$, $-z$), respectively (H···O distances of 2·355 and 2·360 Å).

The zero contours around the non-bonding density peaks in Fig. 6 are flattened toward the corresponding nuclei, away from the hydrogen-bonding directions. Similar shifts of the zero contour have been observed previously in experimental studies (*e.g.* Thomas, 1977; Tellgren, Thomas & Olovsson, 1977; Legros & Kvick, 1980; Eisenstein, 1979; Eisenstein & Hirshfeld, 1983) and in theoretical computations for hydrogen-bonded systems (*e.g.* Yamabe & Morokuma, 1975; Eisenstein & Hirshfeld, 1983).

The deformation density in the plane of the water molecule and in a perpendicular plane through the H—O—H angle bisector is shown in Fig. 7. The non-bonding density peak near O*W* is much wider in the out-of-plane direction than in the molecular plane, in accord with the conventional picture of two lone pairs above and below the molecular plane. The zero contour around the non-bonding peak in Fig. 7(*b*) is

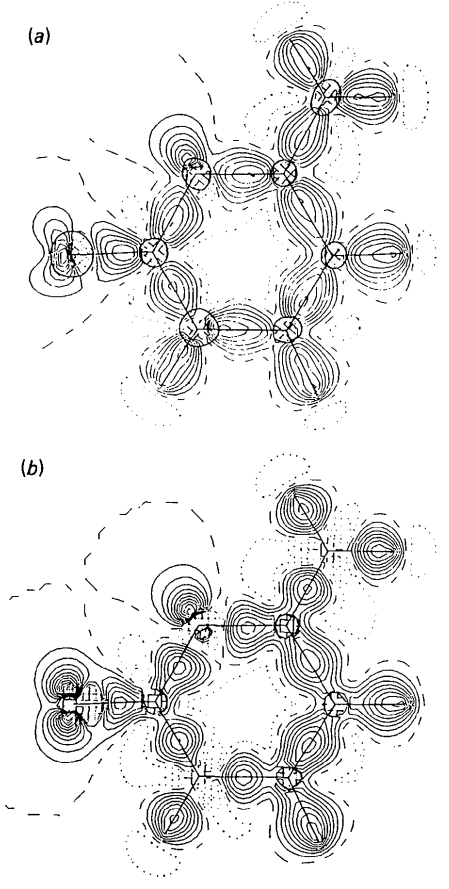

Fig. 3. The deformation density in the molecular plane of cytosine. Positive contours denoted by solid lines; negative contours dotted; zero contour dashed. Contour interval 0·1 e Å^{-3}. The heavy contours enclose regions with $\sigma(\delta\rho) > 0{\cdot}1$ e Å^{-3}. (*a*) Experimental, (*b*) 4-31G**.

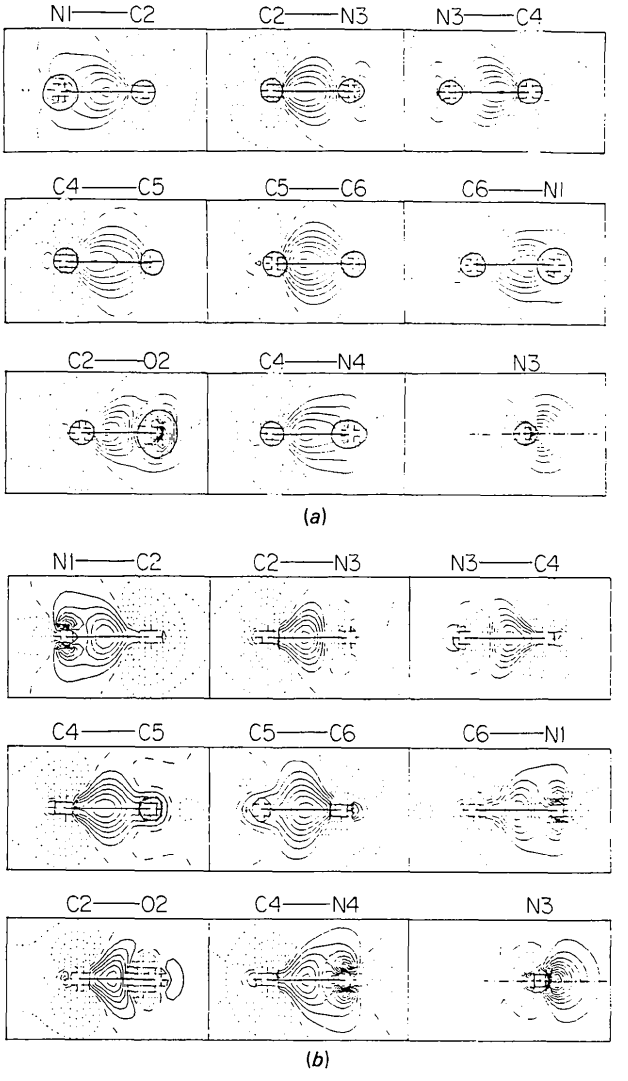

Fig. 4. The deformation density in sections through bonds, perpendicular to the molecular plane of cytosine. Contours as in Fig. 3. (*a*) Experimental, (*b*) 4-31G**.

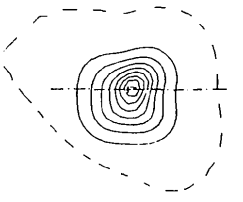

Fig. 5. The experimental deformation density in a section perpendicular to the C2—O2 bond in cytosine, 0·1 Å behind the O atom. The molecular plane is horizontal. Contours as in Fig. 3.

displaced toward the O-atom position as observed for the other hydrogen bonds in this structure (Fig. 6).

Refinement for 9-methyladenine

The results of the low-temperature neutron diffraction study for 9-methyladenine (McMullan, Benci & Craven, 1980) served as a starting point in a deformation refinement against the low-temperature (~126 K) X-ray data of Craven & Benci (1981), which included 4002 reflections with $F > 3\sigma(F)$. The H-atom positions were described in local coordinate systems as for cytosine monohydrate. The X—H bond lengths were fixed at their values from the neutron study except that the methyl-H-atom positions were constrained to threefold symmetry about the C9—N9 axis.

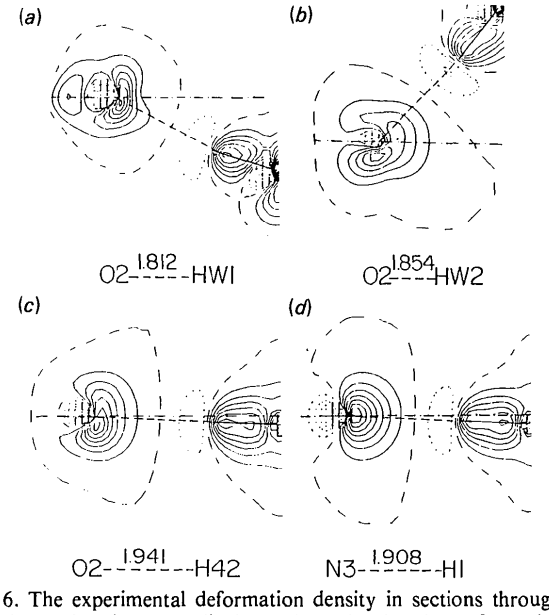

Fig. 6. The experimental deformation density in sections through hydrogen bonds, perpendicular to the molecular plane of cytosine (horizontal). Contours as in Fig. 3. (*a*) O2···H*W*1(x, $\frac{1}{2}-y$, $\frac{1}{2}+z$), (*b*) O2···H*W*2(x, y, z), (*c*) O2···H42($-x$, $-\frac{1}{2}+y$, $\frac{1}{2}-z$), (*d*) N3···H1($-x$, $\frac{1}{2}+y$, $\frac{1}{2}-z$). Distances in Å.

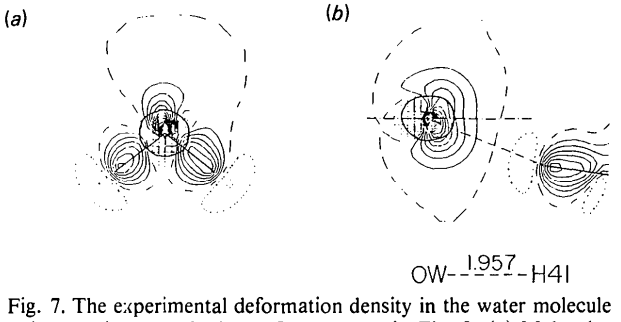

Fig. 7. The experimental deformation density in the water molecule in cytosine monohydrate. Contours as in Fig. 3. (*a*) Molecular plane, (*b*) perpendicular section through the H—O—H angle bisector showing the hydrogen bond. Distance in Å.

Table 6. *9-Methyladenine – internal mean-square displacements for* H *atoms* (Å^2)

	Stretching	In-plane bending	Out-of-plane bending
H2	0·0062	0·0114	0·0207
H8	0·0047	0·0137	0·0238
H61	0·0053	0·0115	0·0037
H62	0·0048	0·0084	0·0166
HMe*	0·0072	0·0183	0·0532

* For HMe 'in-plane' and 'out-of-plane' refer to the local N—C—H plane; the out-of-plane component is mainly due to methyl torsion.

The thermal vibrations of the H atoms in 9-methyladenine were estimated as for cytosine monohydrate. The rigid-body parameters for the 11 C,N skeleton atoms were derived in a separate constrained refinement. The mean-square internal displacements were obtained by subtracting the contributions of the rigid-body motion from their U_{ij} in the neutron study and resolving the residual motion into stretching, in-plane and out-of-plane bending amplitudes (Table 6). The parameters for the CH_3 H atoms were averaged. These H atoms have large torsion amplitudes about the C9—N9 axis.

The low cutoff in the X-ray data for 9-methyladenine ($S_{max} = 2{\cdot}0$ Å^{-1}) dictated a restricted initial deformation model. This included nine deformation types for the C,N atoms and one for the H atoms. N1 and N3 had a common deformation type and so did C4 and C5. The deformations of the C,N atoms had *mm* symmetry, except for C9, where *3m* symmetry was more appropriate. The coefficients of the cusp deformations for these atoms were fixed at 0. The H atoms were contracted to an effective charge of $\zeta = 1{\cdot}2$; their deformations had axial symmetry and were limited to $n \leq 3$, as in the refinement for cytosine monohydrate. With this model 233 parameters were refined: 99 positional and vibrational parameters for the C,N atoms and ten coordinates for the H atoms, 120 deformation coefficients, three α_a, one for each group C,N,H, and a scale factor. As the refinement proceeded it appeared that for strong reflections $F_o < F_c$ as if the extinction correction applied to the original data was too small (Craven & Benci, 1981). Thus, an additional isotropic extinction correction was applied, as for cytosine monohydrate, with $c = 0{\cdot}0007$. The magnitudes of Δ, averaged over small intervals in F, increased smoothly with F. Therefore, a correction linear in F^2 was added to the estimated variances $\sigma^2(F^2)$. The weights of the strong reflections were further reduced because of the approximate extinction correction. The corrected variances had the form: $\sigma^2(F^2) = \sigma^2(F_o^2) + (0{\cdot}032F^2)^2 + (0{\cdot}0021F^2)^4$, where $\sigma^2(F_o^2)$ is the variance estimated by Craven & Benci. The agreement factors with this model were $R = 0{\cdot}0356$, $wR = 0{\cdot}0738$ and $G = 0{\cdot}920$.

Table 7. *9-Methyladenine – anisotropic thermal parameters* $\times 10^4$ (Å^2) *for the* C *and* N *atoms*

Atom labels are indicated in Fig. 2(*c*).

	U_{11}	U_{22}	U_{33}	U_{12}	U_{13}	U_{23}
N1	196 (2)	132 (2)	107 (2)	−7 (1)	91 (2)	−4 (1)
C2	203 (3)	142 (2)	113 (2)	0 (2)	91 (2)	16 (1)
N3	195 (3)	123 (2)	132 (2)	9 (1)	91 (2)	26 (1)
C4	146 (2)	104 (2)	116 (2)	0 (1)	74 (2)	4 (2)
C5	165 (2)	99 (2)	108 (2)	−2 (1)	83 (2)	0 (2)
C6	169 (3)	107 (2)	107 (2)	−3 (1)	85 (2)	−2 (1)
N6	298 (3)	101 (2)	150 (2)	8 (2)	150 (2)	4 (1)
N7	237 (3)	115 (2)	128 (2)	0 (1)	122 (2)	−1 (2)
C8	228 (3)	122 (2)	149 (2)	−1 (2)	123 (2)	−14 (2)
N9	183 (2)	105 (2)	145 (2)	7 (1)	100 (2)	−3 (1)
C9	263 (3)	110 (2)	225 (3)	25 (2)	136 (2)	2 (2)

Several changes in the deformation model have been tested. With separate types for C4 and C5, *wR* decreased slightly but significantly to 0·0736. A similar small drop in *wR* occurred when N1 and N3 were assigned separate types. Lowering the symmetry of the deformations from *mm* to *m* for C2, N3, C6 or N9 had negligible effects on *wR*. However, similar changes for N1, C4, C5, N6, N7 or C8 lowered *wR*. Local *lm* mirror planes were retained for the deformations of these atoms, except for N6, whose deformations had a local *ln* mirror plane. Relaxation of the latter constraint had no effect on *wR*. The α_a parameters diverged when the symmetry constraints were relaxed; therefore they were fixed at their values from the initial refinement. In the last few cycles the α_a were refined in a separate block, but their values did not change much. Refining the coefficients of the cusp deformations under the cusp constraint produced high deformation density peaks at the atomic centers and an insignificant change in *wR*. These parameters were fixed at zero. The final number of refined parameters was 308, giving $R = 0{\cdot}0343$, $wR = 0{\cdot}0714$ and $G = 0{\cdot}898$.

Structure and deformation density of 9-methyladenine

Atomic positions and thermal vibrations

The atomic coordinates from the deformation refinement are very similar to those from the neutron diffraction experiment (McMullan, Benci & Craven, 1980). Discrepancies about twice the sum of the standard deviations from the two refinements occur for *the x coordinates of* N1 *and* C5.

The U_{11} values in Table 7 deviate from the corresponding values from the neutron study by more than twice the sum of the standard deviations, for all atoms except C8 and C9. Craven & Benci (1981) report a similar discrepancy for U_{11} and U_{33} between their pseudo-atom refinement against the X-ray data and the neutron diffraction results. The U_{11} parameters in Table 7 have intermediate values, larger than those for the pseudo-atom refinement and smaller than those from the neutron study. The U_{22} and U_{33} in Table 7 are very close to the neutron diffraction results, except for U_{22}(N9), U_{22}(C5) and U_{33}(N9), where the deviation is very slightly larger than twice the sum of the standard deviations from the two experiments.

Table 8. *9-Methyladenine – mean-square displacements of bonded atoms along the bonds* $\times 10^4$ (Å^2)

R.m.s. difference 0·00034 Å^2.

$A-B$ bond	Z_A^2	Z_B^2	$A-B$ bond	Z_A^2	Z_B^2
N1–C2	132	131	C6–N6	109	103
C2–N3	149	149	C5–N7	94	93
N3–C4	112	107	N7–C8	115	116
C4–C5	102	99	C8–N9	137	129
C5–C6	97	100	C4–N9	113	111
N1–C6	93	93	N9–C9	106	107

The mean-square displacements of bonded atoms along the bonds are listed in Table 8. The r.m.s. difference is 0·00034 Å^2, similar to the corresponding value from the neutron diffraction experiment, 0·00031 Å^2. Both are larger than the corresponding r.m.s. difference for cytosine monohydrate (Table 3), in accordance with the larger variances (Table 7).

Experimental deformation density

The experimental static deformation density in the mean molecular plane of 9-methyladenine is plotted in Fig. 8(*a*). Regions where $\sigma(\delta\rho) > 0{\cdot}1$ e Å^{-3} are surrounded by heavy contours. At the NH_2 H-atom positions $\sigma(\delta\rho) = 0{\cdot}09$ e Å^{-3}. At the bond peaks $\sigma(\delta\rho) = 0{\cdot}04$ e Å^{-3}, except for the C2–H2 and C6–N6 bonds where it reaches 0·05 e Å^{-3}. At the center of the five-membered ring $\sigma(\delta\rho) = 0{\cdot}03$ e Å^{-3}, whereas at the center of the six-membered ring it is 0·02 e Å^{-3}.

Partitioning into atomic fragments and integration have been carried out as for cytosine monohydrate, except that for 9-methyladenine it was not necessary to use a finer grid near the atomic positions. Atomic multipole moments are listed in Table 9.

The deformation density in Fig. 8(*a*) shows bonding peaks for all bonds and a non-bonding peak near each of the –N= atoms. These atoms have large dipole moments that point away from their non-bonding peaks (Table 9) and their density expands in this direction. Similar characteristics have been noted above for –N3= in cytosine monohydrate. N1 and N7 are more negative than N3, in agreement with the monopole populations listed by Craven & Benci and with these being preferred hydrogen-bonding sites (Craven & Benci, 1981).

Sections through bonds and perpendicular to the molecular plane are presented in Fig. 9(*a*). Most C–C and C–N bond peaks are appreciably wider in the out-of-plane direction than in the mean plane. Perpendicular sections through the non-bonding density peaks of N1, N3 and N7 (Fig. 9*a*) show localization of $p\pi$ density near these atoms. However, unlike N1 and N7, N3 has a positive μ_{nn}, indicating contraction

compared to a free N atom. Negative deformation densities occur above and below the C atoms (Fig. 9*a*), as in cytosine, except near C5. The density above and below this atom is slightly positive, as in the corresponding theoretical map (Fig. 9*b*).

The deformation densities above and below N6 and N9 (Fig. 9*a*) are positive, as for the $-NH_2$ and $-NH-$ N atoms in cytosine. The peak above N6 in Fig. 9(*a*) is considerably higher than the peak below it, even in view of the high standard deviation for $\delta\rho$ in this region, in accordance with a slight pyramidalization of N6. The higher peak occurs on the side opposite to the positions of H61 and H62, which deviate by 0·275 and 0·087 Å, respectively, in the same sense from the mean plane of the C,N atoms. The NH_2 N atom also deviates from this mean plane, in the same direction as the H atoms, by only 0·047 Å. This atom has a considerable dipole component in the *n* direction in accord with the asymmetry in the maps.

The H atoms are positive. However, the $-NH_2$ H atoms have much higher charges than the $-CH-$ and $-CH_3$ H atoms, as was noted above for cytosine monohydrate. Similarly, the monopole populations that Craven & Benci (1981) obtained for the $-CH-$ and $-CH_3$ H atoms are very close to 1·0, while for the NH_2 H atoms these populations are smaller, indicating positive charges. The H atoms have negative μ_l (Table 9), whose magnitudes are larger for the $-NH_2$ H atoms than for those attached to C atoms.

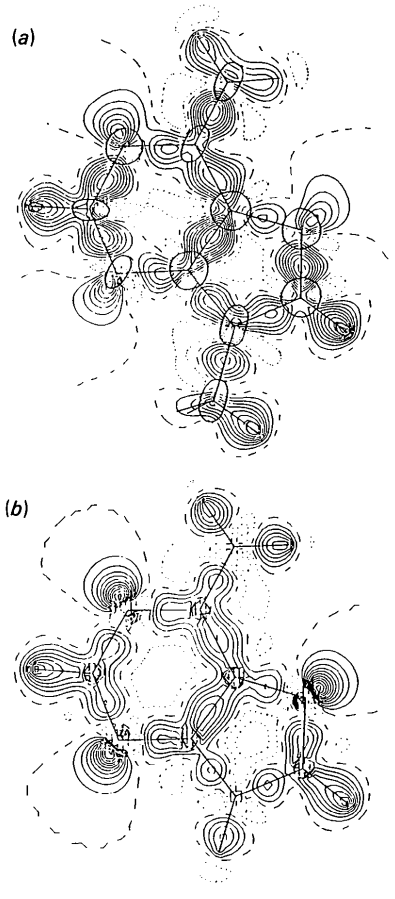

Fig. 8. The deformation density in the molecular plane of (*a*) 9-methyladenine (experimental), (*b*) adenine (4-31G). Contours as in Fig. 3.

Table 9. *9-Methyladenine – experimental and theoretical (Eisenstein, 1988) atomic multipole moments* $\times 10^3$ (e, e Å, e Å^2)

Local coordinate systems are indicated in Fig. 2(*c*).

	Basis	q	μ_l	μ_m	μ_n	μ_{ll}	μ_{mm}	μ_{nn}	μ_{lm}	μ_{ln}	μ_{mn}
N1	Exp.	−280	137	39	4	−42	31	−25	−7	−2	2
	4-31G	−249	230	24	0	−108	22	−61	−10	0	0
C2	Exp.	−18	29	−18	4	110	1	130	22	2	−1
	4-31G	105	19	0	0	115	8	128	2	0	0
N3	Exp.	−166	100	−57	2	−26	31	32	11	1	2
	4-31G	−248	230	−10	0	−119	17	−58	0	0	0
C4	Exp.	106	−16	−59	−4	115	66	151	26	1	0
	4-31G	82	−26	−25	0	80	25	83	−3	0	0
C5	Exp.	−15	−15	18	2	72	80	102	−5	2	−5
	4-31G	−50	−27	−15	0	51	69	27	4	0	0
C6	Exp.	150	16	−19	−8	105	84	207	−2	−12	2
	4-31G	156	−25	−3	0	64	51	123	−15	0	0
N6	Exp.	−133	−2	−3	57	90	134	40	−3	−23	−4
	4-31G	−150	21	5	0	76	88	−57	3	0	0
N7	Exp.	−254	154	−24	−2	−115	10	−34	−11	3	1
	4-31G	−230	228	−18	0	−126	10	−63	6	0	0
C8	Exp.	7	−27	63	−2	93	62	184	−23	−2	−1
	4-31G	80	1	32	0	108	55	100	3	0	0
N9	Exp.	−50	−54	−11	7	48	95	65	−2	−1	−2
	4-31G	−71	9	3	0	77	67	−23	1	0	0
H2	Exp.	41	−91	−16	−2	82	51	60	−2	0	0
	4-31G	53	−81	1	0	72	66	73	0	0	0
H61	Exp.	180	−113	22	2	104	89	104	−15	7	3
	4-31G	140	−105	11	0	86	89	70	−9	0	0
H62	Exp.	185	−123	13	−8	116	95	98	−6	−11	−7
	4-31G	137	−107	13	0	89	82	68	−5	0	0
H8	Exp.	47	−86	25	−5	85	68	83	−1	1	0
	4-31G	68	−87	−1	0	76	85	75	3	0	0
C9	Exp.	−75	14	19	9	175	183	176	2	1	−5
H91	Exp.	89	−104	−13	0	94	98	98	2	1	0
H92	Exp.	94	−105	−12	−2	96	97	94	3	−1	−1
H93	Exp.	90	−104	−14	4	95	96	89	3	−1	2
H9	4-31G	173	−115	−4	0	96	98	79	0	0	0

Sections through the hydrogen bonds N1···H61(x, $\frac{1}{2}-y$, $\frac{1}{2}+z$) and N7···H62(x, $\frac{1}{2}-y$, $-\frac{1}{2}+z$) show that the non-bonding peaks near N1 and N7 are symmetric, except that the zero contours are shifted slightly toward the N positions (Fig. 10). The effect is smaller than the corresponding one in cytosine monohydrate (Fig. 6).

The deformation density in Fig. 8(*a*) is very similar to the $\delta\rho$ obtained by Craven & Benci (1981; Fig. 3*b*). In both maps the highest bond peak occurs for C4–C5. It reaches 0·85 (4) e Å^{-3} in Fig. 8(*a*) and 0·73 (5) in the map by Craven & Benci. Also in both maps the N3–C4, C5–N7 and C6–N1 bond peaks are considerably lower than other C–N bond peaks. The deformation density maps in planes parallel to the mean molecular plane presented by Craven & Benci (1981; Figs. 3*a,c*), imply larger out-of-plane extension of the C2–N3, C4–C5 and N7–C8 bond peaks than for other bonds, and show negative regions above and below C2, C4, C6 and C8, as in Fig. 9(*a*). Their maps also hint at a slight asymmetry near N6.

The similarity of the $\delta\rho$ maps from the present deformation refinement and from the pseudo-atom

refinement by Craven & Benci (1981) is interesting, because two different formalisms have been used for modelling the chemical bonding effects. However, the thermal parameters from the present deformation refinement are closer to the neutron diffraction results than are those from the pseudo-atom refinement and our residual $F_o - F_c$ maps (not presented) do not show features exceeding 0·2 e Å^{-3}, suggesting a small advantage of Hirshfeld's deformation model. It seems that in both refinements the thermal vibration parameters absorbed much of the model error.

Comparison with theoretical deformation densities

In comparing experimental and theoretical deformation densities one should consider several sources of discrepancies. The experimental deformation densities suffer from errors in the data and from limitations of the model, while the theoretical maps are affected by the Hartree–Fock approximation and the shortcomings of the basis set. Moreover, in this study the compared entities are not identical. The molecules in the crystal are perturbed by hydrogen bonding while the computations have been carried out for isolated molecules (Eisenstein, 1988). In addition, the experimental deformation density in 9-methyladenine is compared with $\delta\rho$ in the unsubstituted adenine molecule computed at the 4-31G level owing to computing time limitations.

The effects of adding polarization functions to the basis set and the effects of substituting CH_3 for H have been discussed before (Eisenstein, 1988). Thus, polarization functions do not affect the net atomic charges. However, they cause transfer of charge from non-bonding regions to the bonds. Hence, atomic dipole moments for atoms that bear non-bonding density peaks decrease by 0·08 e Å on adding polarization functions to the basis set. The second moments μ_{nn} increase for all C,N atoms on enlarging the basis, by ~ 0·02 e Å^2. Methyl substitution causes electronic charge to be pushed into the ring and the C–CH_3 group is less negative than the corresponding –CH– group. The substituted ring C atom is less negative than the unsubstituted atom by 0·05 e, because it is bonded to a negative methyl C atom. The dipole component, directed into the ring, of the ring C atom decreases by 0·01 e Å on substitution and its second moment in this direction decreases by 0·03 e Å^2.

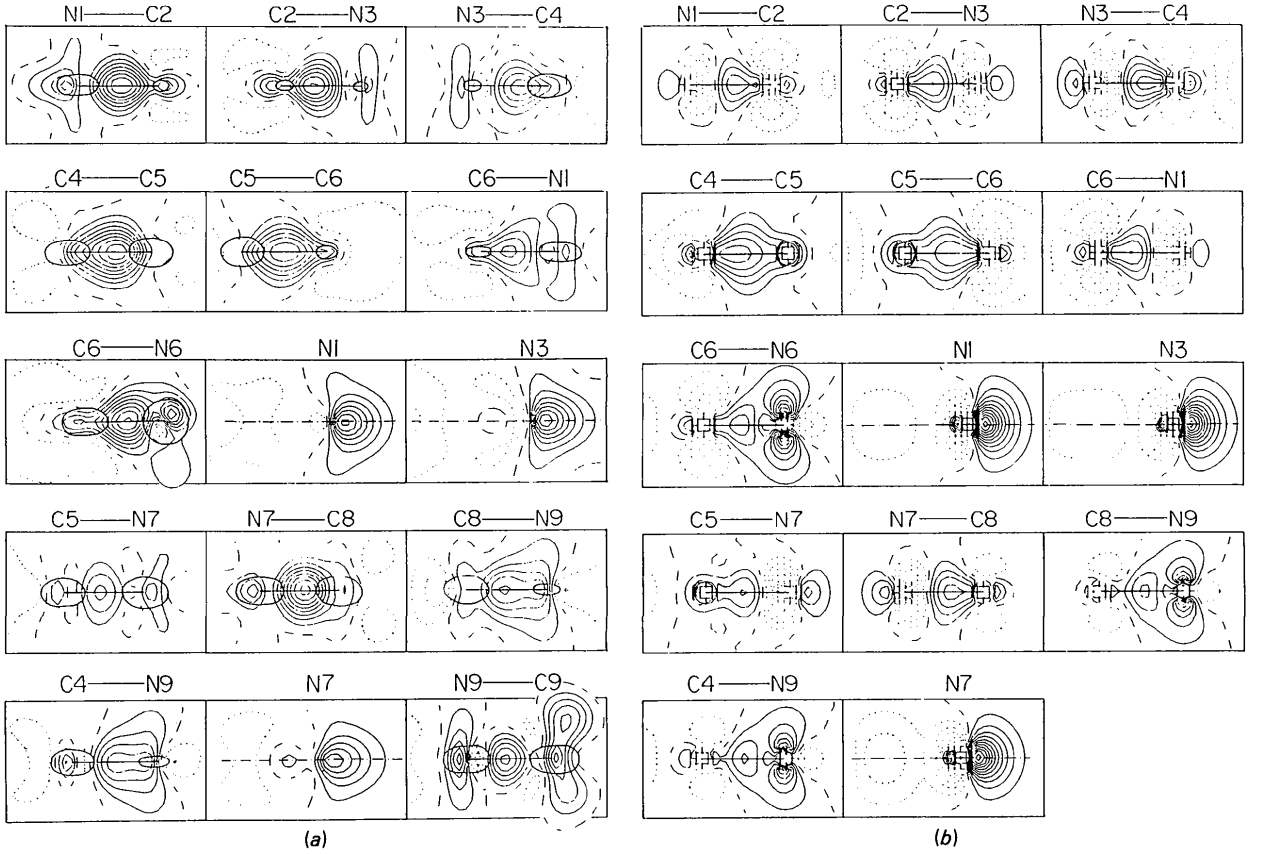

Fig. 9. The deformation density in sections through bonds, perpendicular to the molecular plane of (*a*) 9-methyladenine (experimental); (*b*) adenine (4-31G). Contours as in Fig. 3.

The effects of hydrogen bonding on the deformation density are illustrated by the comparison of the formic acid monomer with its cyclic dimer (Eisenstein & Hirshfeld, 1983). They are mostly confined to the carbonyl O and hydroxyl H atoms and are largely attributable to the superposition of the monomer deformation densities in the hydrogen-bond regions. The carbonyl O atom in the dimer is less negative by 0·031 e than in the monomer and its dipole moment is smaller by 0·02 e Å. In the formic acid monomer the dipole of the carbonyl O atom points in the O–C direction. The hydrogen bond in the cyclic dimer is directed toward one O lobe and is not symmetric with respect to the O–C axis. Thus, the direction of the dipole changes; in the dimer μ_l(O) (Fig. 2*d*) is smaller by 0·045 e Å than in the monomer while the perpendicular component, μ_m(O), is larger by 0·070 e Å. The oxygen second moments μ_{ll} and μ_{mm} increase on dimerization by 0·045 and 0·056 e Å^2, respectively. The corresponding increase for μ_{nn} is smaller, 0·013 e Å^2. The hydroxyl H atom loses 0·044 e of its positive charge on dimerization. Its dipole moment, which points into the O–H bond, decreases by 0·08 e Å without changing direction. The positive second moments of the hydroxyl H atom are smaller in the dimer than in the monomer. The change for μ_{ll}, 0·07 e Å^2, is larger than in the transverse directions, 0·025 e Å^2. The carbonyl C atom in formic acid is much less affected by hydrogen bonding than the carbonyl O and hydroxyl H atoms.

Cytosine

The experimental $\delta\rho$ maps in the molecular plane of cytosine and in the perpendicular planes closely resemble the corresponding theoretical 4-31G** maps in positions, shapes and heights of most peaks and troughs (Figs. 3, 4). They are much closer to the 4-31G** results than to maps computed with smaller bases (Eisenstein, 1988). Discrepancies between the experimental and 4-31G** maps occur in non-bonding regions, where the experimental peaks are lower. This is due, in part, to the fact that in the theoretical maps the non-bonding maxima occur very close to the corresponding nuclei, where the deformation model is evidently deficient and $\sigma(\delta\rho)$ is high. These maxima are closer to the O than to the N nuclei, thus rationalizing the difficulty in refining the α_a for O atoms. Probably for the same reason, the difference between the heights of the O2 non-bonding peak in the experimental and 4-31G** maps is much larger than the corresponding difference for N3. This may also be related to the fact that O2 accepts three hydrogen bonds and N3 only one.

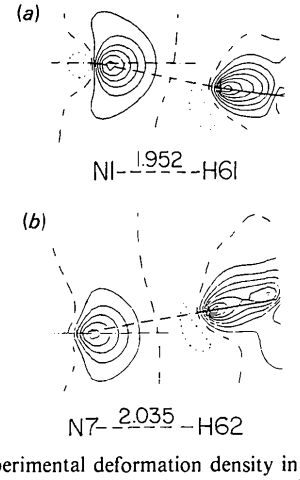

Fig. 10. The experimental deformation density in sections through hydrogen bonds, perpendicular to the molecular plane of 9-methyladenine. Contours as in Fig. 3. (*a*) N1···H61(x, $\frac{1}{2}-y$, $\frac{1}{2}+z$), (*b*) N7···H62(x, $\frac{1}{2}-y$, $-\frac{1}{2}+z$). Distances in Å.

A quantitative comparison between experiment and theory for cytosine is presented in Table 4. The experimental net atomic charges of the ring atoms have alternating signs. Thus, C2, C4 and C6 are positive while N1, N3 and C5 are negative, as observed for all six-membered rings in the theoretical computations for DNA bases (Eisenstein, 1988). However, the absolute values of the experimental charges for cytosine are smaller than the 4-31G** values, except for N1.

The signs of the experimental and theoretical μ_l and μ_m dipole components are the same for all atoms except a few very small components. The differences in the magnitudes of μ_m are usually small; the largest occurs for C6 (0·023 e Å). The experimental μ_{nn} terms for all C,N,O atoms except C2 are more positive than the respective 4-31G** values.

Many of the differences between the experimental and 4-31G** multipole moments are attributable to hydrogen bonding. Thus, the experimental charges and μ_{ll} moments of the hydrogen-bond acceptors N3 and O2 are less negative than the 4-31G** values and their μ_l dipoles are smaller (Table 4). For N3 the differences are quantitatively similar to the corresponding ones in the comparison of formic acid dimer and monomer. Also, the difference between the experimental and theoretical μ_{nn}(N3) is slightly larger than the average, possibly another effect of hydrogen bonding. For O2 the differences between the experimental and 4-31G** charges and μ_{mm} moments are much larger than the corresponding values for formic acid, whereas the differences for μ_l and μ_{ll} are smaller.

The differences between the experimental and 4-31G** multipole moments for H1, H41 and H42 are very similar. Their experimental charges and second moments are lower than the theoretical values and their μ_l dipoles are less negative, as expected from the comparison of the hydroxyl H-atom moments in formic acid dimer and monomer. H5 and H6, which participate only in very weak hydrogen bonds, are affected similarly to the –NH– and –NH_2 H atoms, probably

Table 10. *Molecular dipole and quadrupole moments, referred to the centers of mass*

The molecular coordinate systems are indicated in Fig. 2. The theoretical values for cytosine and adenine are from Eisenstein (1988). The quadrupole moments θ_{ij} are related to the corresponding second moments μ_{ij} by the relations: $\theta_{xx} = \mu_{xx} - (\mu_{yy} + \mu_{zz})/2$ *etc.*, and $\theta_{xy} = 3\mu_{xy}/2$ *etc.* Molecular dipole moments are given in debye (1 debye $\equiv 3{\cdot}336 \times 10^{-30}$ C m) and quadrupole moments in Buckingham (1 Buckingham $\equiv 3{\cdot}336 \times 10^{-40}$ C m^2).

Molecule	Basis	μ_x	μ_y	μ_z	θ_{xx}	θ_{yy}	θ_{zz}	θ_{xy}	θ_{xz}	θ_{yz}
Cytosine	STO-3G	5·69	−1·55	0·00	−9·82	13·77	−3·95	6·58	0·00	0·00
	Double-ζ	8·77	−2·17	0·00	−15·16	21·36	−6·19	7·75	0·00	0·00
	4-31G	8·48	−2·00	0·00	−14·11	20·50	−6·39	7·02	0·00	0·00
	4-31G**	8·03	−1·63	0·00	−13·41	20·28	−6·87	6·98	0·00	0·00
	Exp.	5·74	−1·14	0·14	−8·03	11·29	−3·27	6·90	−0·24	0·25
	Exp.(H)[a]	5·99	−3·41	0·23	−11·35	15·28	−3·93	13·73	−0·58	0·11
Water	4-31G**	0·00	−2·18	0·00	2·26	−0·02	−2·24	0·00	0·00	0·00
	Exp.	−0·06	−1·58	−0·01	0·99	−0·12	−0·87	−0·18	0·02	−0·02
	Exp.(H)[a]	−0·06	−2·46	−0·01	1·94	−0·08	−1·86	−0·20	0·02	−0·02
Adenine	4-31G	2·05	−1·46	0·00	−10·43	19·86	−9·43	−4·09	0·00	0·00
	4-31G[**][b]	1·95	−1·15	0·00	−9·57	20·15	−10·58	−3·28	0·00	0·00
	Exp.[c]	2·00	−0·94	−0·77	−20·58	31·59	−11·01	1·70	−1·13	−3·55
9-Methyl-adenine	Exp.	1·74	−1·43	−0·79	−21·84	33·60	−11·77	2·71	−1·14	−3·51

Notes: (*a*) Experimental moments corrected for the estimated effects of hydrogen bonding in the crystal. (*b*) 4-31G[**] molecular moments have been calculated from the 4-31G atomic moments adjusted for the estimated effects of polarization functions (Eisenstein, 1988). (*c*) The experimental molecular moments for adenine have been estimated from the atomic moments of 9-methyladenine with the CH_3 group replaced by H9. The negative charge on N9 was increased by 0·05 e to offset the effect of substitution. The charge on H9 was determined by molecular neutrality and its dipole and second moments were taken from the 4-31G computation.

as a result of the constraints imposed on the deformation model.

As mentioned above, the experimental μ_{nn} for the C,N,O atoms, except C2, are larger than the corresponding 4-31G** values. A similar relative contraction has been observed in the comparison of the experimental deformation density of diformohydrazide with the theoretical deformation density of formamide (Eisenstein, 1979). This recalls the increase in the μ_{nn} of the C,N,O atoms on adding polarization functions to the basis set, that has been observed in the comparison of the 4-31G** with the 4-31G deformation density of cytosine (Eisenstein, 1988) and in the comparisons of the extended-double-ζ densities of formamide (Eisenstein, 1979) and formic acid (Eisenstein & Hirshfeld, 1983) with the corresponding double-ζ densities. Possibly, the difference between the experimental and 4-31G** μ_{nn} in cytosine reflects a remaining inadequacy in the polarization functions contained in the 4-31G** and analogous extended-double-ζ basis sets. It may also indicate a systematic bias caused by the deformation model.

The carbonyl C2 atom in cytosine does not compare well with theory. Its experimental charge is smaller than the 4-31G** value, contrary to the expected effect of hydrogen bonding. For this atom the experimental μ_{nn} is not larger than the theoretical value, as for the other ring atoms.

The molecular dipole and quadrupole moments for cytosine (Table 10) have been calculated from the atomic moments in Table 4. This molecular dipole, 5·8 debye, is smaller than the estimated experimental value, 7·0 debye (Kulakowska, Geller, Lesyng, Bolewska & Wierzchowski, 1970) and also smaller than the theoretical values, except for the STO-3G dipole. This difference may be due to the influence of the hydrogen bonds on the atomic moments. Thus, when the experimental multipole moments of O2, N3, H1, H41 and H42 are corrected for the estimated effects of hydrogen bonding, the molecular dipole of cytosine increases to 6·9 debye, close to the value presented by Kulakowska *et al.* The experimental quadrupole moments have identical signs but smaller magnitudes than the corresponding theoretical moments, indicating similar anisotropy of the molecular charge distributions. When corrected for the estimated effects of hydrogen bonding, their magnitudes increase and are closer to the theoretical values (Table 10).

Water

Fig. 7 compares well with the static theoretical deformation density of free water, calculated with an extended basis set (Hermansson & Lunell, 1982). The O non-bonding peak is narrow in the molecular plane and much wider in the out-of-plane direction. In the theoretical map it has two maxima above and below the molecular plane, very close to the O nucleus, where $\sigma(\delta\rho)$ in the experimental map is high. The experimental map reproduces nicely the deep trough below the O on the molecular twofold axis, but the negative $\delta\rho$ regions, delimiting the non-bonding peak in the $+m$ and $-m$ directions, are much shallower in Fig. 7(*a*) than in the computation. The O—H bond peaks and the troughs

behind the H atoms are similar in the experimental and theoretical maps.

The experimental net charge on O*W* is less negative than the 4-31G** value (Table 5). The difference is in the expected direction for a hydrogen-bond acceptor but larger than the corresponding effect in formic acid. However, the higher moments on O*W* are only slightly influenced by hydrogen bonding. This can be related to the long O*W*···H41 distance (1·957 Å), the weakest intermolecular interaction in the cytosine monohydrate crystal. The difference between the experimental and theoretical charges on O*W* may be due to limitations of the deformation model and to unidentified systematic errors in the data, which affect the sharp $\delta\rho$ features near the O atoms more than other regions in the map. The deformation density near O2 probably suffers from the same errors. Thus, the difference between the experimental and theoretical charges on this atom is due only partly to hydrogen bonding. This smaller effect is in accord with the magnitudes of the effects of hydrogen bonding on the dipole and μ_{ll} of O2.

The differences between the experimental and 4-31G** charges and dipole moments for H*W*1 and H*W*2 are quantitatively similar to the corresponding differences for the hydroxyl H atom in formic acid dimer and monomer. The differences for the second moments are larger in the former comparison but $\Delta\mu_{ll} \gg \Delta\mu_{mm}, \Delta\mu_{nn}$ in both.

The molecular dipole moment of H_2O, calculated from the atomic charges and dipole moments in Table 5, is 1·58 debye and it points from O to H, approximately along the H–O–H angle bisector. This dipole is in the right direction but smaller than both the experimental value, 1·85 debye, and the 4-31G** value, 2·18 debye. Correction of the atomic multipole moments in Table 5 to offset the estimated effects of hydrogen bonding produces an overestimated molecular dipole of 2·5 debye, but brings the molecular quadrupole moments closer to the 4-31G** values (Table 10).

Adenine

The experimental deformation density for 9-methyladenine generally resembles the 4-31G map for adenine (Fig. 8). In both maps the C4–C5 bond has the highest peak, but this is higher by ~0·3 e Å^{-3} in the experimental than in the theoretical map. The other bond peaks are also higher in the experimental map, by 0·05 to 0·4 e Å^{-3}. Most of these differences are attributable to the shortcomings of the 4-31G basis set because in a 4-31G** map the bond peaks are expected to increase by ~0·2 e Å^{-3} (Eisenstein, 1988). Enlarging the basis will also decrease the heights of the 4-31G σ non-bonding peaks near N1, N3 and N7 by ~0·1 e Å^{-3} and flatten the troughs near these atoms. This will improve the agreement between Figs. 8(*a*) and 8(*b*) in these regions but less than for the bond peaks. The positions and shapes of the other troughs are similar in the experimental and theoretical maps.

Negative $\delta\rho$ regions occur above and below the C atoms in Figs. 9(*a*) and 9(*b*). In both maps these features are most pronounced near C6. However, the troughs in the 4-31G maps are deeper than those in the experimental maps. N6 and N9 have positive $\delta\rho$ peaks near them above and below the molecular plane. These features too are more conspicuous in the 4-31G map than in the experimental map. The differences will be smaller in a comparison with a 4-31G** map.

A quantitative comparison between experiment and theory is presented in Table 9. The 4-31G charges in the six-membered ring in adenine have alternating signs. The situation in 9-methyladenine is similar, except that C2 is slightly negative, almost neutral. A similar large discrepancy between the experimental and theoretical net charges occurs for the other –CH– C atom, C8. The experimental μ_{nn}(C8) is larger than the corresponding 4-31G moment. This discrepancy will be remedied only in part by enlarging the basis to 4-31G** and it occurs for all the C,N atoms in 9-methyladenine, except C2 and C6. A similar trend has been noted above in the comparison for cytosine, where the experimental μ_{nn} values for all the C,N,O atoms except C2 are higher than the corresponding 4-31G** values.

The experimental charges and dipole moments of N1 and N7 are similar to the theoretical values if the latter are corrected for the lack of polarization functions. These moments do not seem to be affected by hydrogen bonding. Furthermore, the small discrepancies between the experimental and theoretical multipole moments of the $-NH_2$ H atoms are opposite to the expected differences for hydrogen-bonded H atoms. However, the experimental μ_{ll} moments of N1 and N7 are less negative than in theory as for other hydrogen-bond acceptors.

N9 is less negative in the experiment than in the 4-31G computation. Also, its μ_l is more negative in the experiment and its μ_{ll} moment is smaller. These effects are qualitatively as expected on replacement of H by CH_3. The N–CH_3 group in 9-methyladenine has a higher net charge than the N9–H9 group in the calculation for adenine, as in the analogous comparison of thymine with uracil (Eisenstein, 1988). Also, the strongly positive experimental μ_{nn}(N9) may be attributed, in part, to the substitution.

The deformation density in the CH_3 group may be compared to the appropriate portions of the theoretical deformation densities for ethane (Eisenstein & Hirshfeld, 1983) and thymine (Eisenstein, 1988). The charge of the methyl C atom in 9-methyladenine (–0·075 e) is similar to the double-ζ value for ethane (–0·069 e) and the 4-31G value for thymine (–0·075 e), but it contracts slightly more (average $\mu_{ii} = 0{\cdot}178$ *versus* 0·120 e Å^2 in ethane and thymine).

The net charges of the methyl H atoms in 9-methyladenine (0·09 e) are higher than in ethane (0·024 e) and thymine (0·034 e) and their dipole moments are more negative, −0·104 *versus* −0·067 e Å in the two theoretical computations. The average experimental μ_{ii} of the methyl H atoms, 0·095 e Å^2, is slightly larger than the corresponding values for ethane (0·066 e Å^2) and thymine (0·071 e Å^2). All these differences are probably due to the limitations of the deformation model, where all the H atoms had a common deformation type, forcing the CH_3 H atoms to be similar to the −CH− and $-NH_2$ H atoms.

The molecular moments for 9-methyladenine and estimated values for adenine have been calculated from the experimental atomic multipole moments in Table 9. They are similar to one another and resemble, qualitatively, the theoretical values for adenine (Table 10).

Summary

This study presents experimental static deformation densities in cytosine monohydrate and in 9-methyladenine and compares them with theoretical deformation densities in cytosine (4-31G**) and adenine (4-31G), respectively. The comparison for cytosine shows quantitative agreement between theory and experiment for most atoms. Moreover, most of the differences can be related semi-quantitatively to the effects of intermolecular hydrogen bonding, as deduced from double-ζ computations for formic acid monomer and dimer.

The agreement between the deformation densities of 9-methyladenine and adenine is qualitative and remains so when the 4-31G deformation density for adenine is corrected for the lack of polarization functions in the basis. This may be attributed to the lower resolution of the X-ray data for 9-methyladenine than for cytosine monohydrate. The effects of substitution of CH_3 for H in adenine are qualitatively similar to those found in the comparison of the theoretical deformation densities of thymine and uracil. Hydrogen bonds have little effect on the deformation density in 9-methyladenine. This may be due to the weak interactions in this crystal, where the H···N distances are 1·952 and 2·034 Å, longer than the H···N (1·908 Å) and most H···O distances (1·812, 1·854, 1·941 and 1·957 Å) in cytosine monohydrate. Similarly, the long H···O*W* interaction in the latter structure has little influence on the deformation density of the water O atom.

I thank Professor Z. Shakked for suggesting the subject and Professor F. L. Hirshfeld for critical reading of the manuscript and very helpful discussion. This study was supported by the Israeli Academy of Sciences and Humanities and by the United States/Israel Binational Science Foundation.

References

BADER, R. F. W. & BEDDALL, P. M. (1972). *J. Chem. Phys.* **56**, 3320–3329.
BADER, R. F. W., BEDDALL, P. M. & PESLAK, J. JR (1973). *J. Chem. Phys.* **58**, 557–566.
BERKOVITCH-YELLIN, Z. & LEISEROWITZ, L. (1980). *J. Am. Chem. Soc.* **102**, 7677–7690.
BERKOVITCH-YELLIN, Z. & LEISEROWITZ, L. (1982). *J. Am. Chem. Soc.* **104**, 4052–4064.
COPPENS, P. (1968). *Acta Cryst.* A**24**, 253–257.
COPPENS, P., LEISEROWITZ, L. & RABINOVICH, D. (1965). *Acta Cryst.* **18**, 1035–1038.
CRAVEN, B. M. & BENCI, P. (1981). *Acta Cryst.* B**37**, 1584–1591.
EISENSTEIN, M. (1979). *Acta Cryst.* B**35**, 2614–2625.
EISENSTEIN, M. (1988). *Int. J. Quantum Chem.* **33**, 127.
EISENSTEIN, M. & HIRSHFELD, F. L. (1983). *Acta Cryst.* B**39**, 61–75.
ERIKSSON, A. & HERMANSSON, K. (1983). *Acta Cryst.* B**39**, 703–711.
HAMILTON, W. C. (1965). *Acta Cryst.* **18**, 502–510.
HAREL, M. & HIRSHFELD, F. L. (1975). *Acta Cryst.* B**31**, 162–172.
HERMANSSON, K. & LUNELL, S. (1982). *Acta Cryst.* B**38**, 2563–2569.
HIRSHFELD, F. L. (1976). *Acta Cryst.* A**32**, 239–244.
HIRSHFELD, F. L. (1977*a*). *Theor. Chim. Acta*, **44**, 129–138.
HIRSHFELD, F. L. (1977*b*). *Isr. J. Chem.* **16**, 226–229.
HIRSHFELD, F. L. & MIRSKY, K. (1979). *Acta Cryst.* A**35**, 366–370.
KULAKOWSKA, I., GELLER, M., LESYNG, B., BOLEWSKA, K. & WIERZCHOWSKI, K. L. (1970). *Biochem. Biophys. Acta*, **407**, 420–429.
LEGROS, J. P. & KVICK, A. (1980). *Acta Cryst.* B**36**, 3052–3059.
MCMULLAN, R. K., BENCI, P. & CRAVEN, B. M. (1980). *Acta Cryst.* B**36**, 1424–1430.
NIEDLE, S., ACHARI, A. & RABINOVITCH, M. (1976). *Acta Cryst.* B**32**, 2050–2053.
SUSI, H., ARD, J. S. & PURCELL, J. M. (1973). *Spectrochim. Acta Part A*, **29**, 725–733.
TELLGREN, R., THOMAS, J. O. & OLOVSSON, I. (1977). *Acta Cryst.* B**33**, 3500–3504.
THOMAS, J. O. (1977). *Acta Cryst.* B**33**, 2867–2876.
WEBER, H. P., CRAVEN, B. M. & MCMULLAN, R. K. (1980). *Acta Cryst.* B**36**, 645–649.
YAMABE, S. & MOROKUMA, K. (1975). *J. Am. Chem. Soc.* **97**, 4458–4456.